Letters in Applied NanoBioScience
Open-Access Journal (ISSN: 2284-6808)

Article
Volume 12, Issue 2, 2023, 45
https://doi.org/10.33263/LIANBS122.045

Investigation on Quantum Computational Analysis and Toxicity Prediction of 4-Nitrophenylisocyanate

Vinayakprasanna N Hegde [1], Jayashankar Jayaprakash [2], Jyothi Kamareddy Raju [3],Chimatahalli S. Karthik [2,*], Puttaswamappa Mallu [2], Kumaraswamy S. Rajashekaramurthy [4,*]

[1] Department of Physics, Vidyavardhaka College of Engineering, Mysuru-570002, Karnataka, India
[2] Department of Chemistry, SJCE, JSS Science and Technology University, Mysuru-570 006, Karnataka, India
[3] Department of Physics, Rao Bahadur Y. Mahabaleswarappa Engineering College, Ballari-583 104, Karnataka, India
[4] Department of Physics, Maharani's Science College for Women, Mysuru-570005, India.
* Correspondence: csk@jssstuniv.in (C.S.K.); 1141srk@gmail.com (S.R.K.);

Scopus Author ID (C.S.K.) 57194565359
Received: 2.01.2022; Accepted: 10.02.2022; Published: 19.03.2022

Abstract: The compound 4-nitrophenylisocyanate is known for its various biological properties and class of compounds in medicinal chemistry. In this paper, we are reporting the DFT studies of 4-nitrophenylisocyanate (NPIC). To better understand molecular properties, the computational study, optimized molecular geometry, and reactive parameters were investigated and calculated by employing the method of DFT and B3LYP/6-311++G(d, p) basis set. The DFT calculations were performed to analyze the frontier molecular orbitals (HOMO-LUMO). The energy difference between HOMO - LUMO is 4.516 eV, and the MEP was traced to find the reactive sites of the compound. In addition, theoretical UV-visible spectrum and vibrational spectra (FT-IR) were obtained in the gas phase using the TD-DFT method. By using pkCSM toxicity of the compound was also predicted. The Quantum Theory of Atoms in Molecules (QTAIM) framework is used to calculate topological parameters. Different intermolecular interactions are described using terms like Reduced Density Gradient (RDG), Non-Covalent Interactions (NCI), electron density, and electron localization function and electron cloud present in the NPIC molecule.

Keywords: NPIC; DFT; UV-Vis; FT-IR; QTAIM.

1. Introduction

Nitrobenzene derivatives (NB) are considered to represent a group of organic compounds with a wide range of pharmaceutical and agricultural applications [1], which are structurally related to natural purine bases and toxic industrial chemical that is used to make explosives, pesticides, and synthetic rubbers, as well as dyes and pharmaceuticals [2]. NB may be breathed, eaten, and absorbed via the skin with ease. Nitrobenzene derivatives possess antimicrobial [3-4], antiamoebic [5], antineoplastic [6], anesthetic [7], anti-inflammatory [8], antibiotics against *Staphylococcus* and *Mycobacterium ranae* [9]. Isocyanates (ICs) significantly impact food and natural product chemistry [10]. Several dietary components and food chemicals contain the isothiocyanate moiety. In addition, many ICs interact with macromolecules of biological relevance, making these compounds relevant for potential therapeutic applications and disease prevention [11]. Due to the electrophilic carbon atom arising from resonance contributions such as RN-C+O- and RN-C+-O–, organic isocyanates (RNCO) are common intermediates in forming natural products [12]. The combined roles of

isocyanate and substituents in the vibration structure of aromatic phenyl isocyanate molecules are of spectroscopic interest after extensive studies on the phenyl isocyanate by many workers [13].

In the present study, we report the optimized structure of the compound 4-nitro phenyl isocyanate. The structure is further carried out for DFT calculations in the gas phase and polarizable continuum model to predict the corresponding spectroscopic data for NPIC molecule, and further QTAIMs analysis was carried out.

2. Materials and Methods

2.1. DFT studies.

All DFT analyses have been performed through Gaussian 09 software. The coordinates of the molecules were optimized using DFT/B3LYP hybrid functional calculations with the 6-311+G (d, p) level basis set in the gas phase. Koopman's approximation was used to calculate the energy gap between the boundary molecular orbitals (HOMO-LUMO), and the corresponding local and global indices (electronegativity, chemical potential, hardness, softness, and electrophilicity) [14-15]. Further, Molecular Electrostatic Potential (MEP) was calculated within the molecular system. All of the output files were visualized by Gaussview 6.0.16 [16]. In addition, the B3LYP/DFT method has been used to assign the vibrational bands to the IR spectrum, and TD-DFT calculations were used to describe the electronic transition for the title compound. Furthermore, non-covalent interactions and RDG calculations of NPIC were analyzed and validated within (QTAIM) using Multiwfn 3.8 and are plotted using the software tool “Visual Molecular Dynamics” (VMD) package.

2.2. Toxicity prediction.

The standard pharmacokinetics were determined for the estimation of the physicochemical and pharmacokinetic parameters in the drug discovery process [17]. The compound NPIC structure is drawn in 2-D structure format using Marvin JS software and then imported into SMILES via the website's interface (http://swissadme.ch/). These compound SMILES were loaded into the pkCSM online tool. [18]. The pkCSM online tool was used for the prediction of toxicity. Using the pkCSM online tool, the Toxicity mode was selected, including AMES toxicity, maximum tolerated dose for humans, oral rat acute toxicity, oral rat chronic toxicity, and minnow toxicity.

3. Results and Discussion

3.1. Geometry optimization and HOMO-LUMO analysis of NPIC.

The optimized molecular structure of NPIC with the numbering of atoms is shown in Figure 1. The optimized structural parameters (bond length and bond angle) by B3LYP/6–311++G (d, p) basis set was shown in Tables 1 and 2. The molecular structure of the NPIC compound is in planar form.

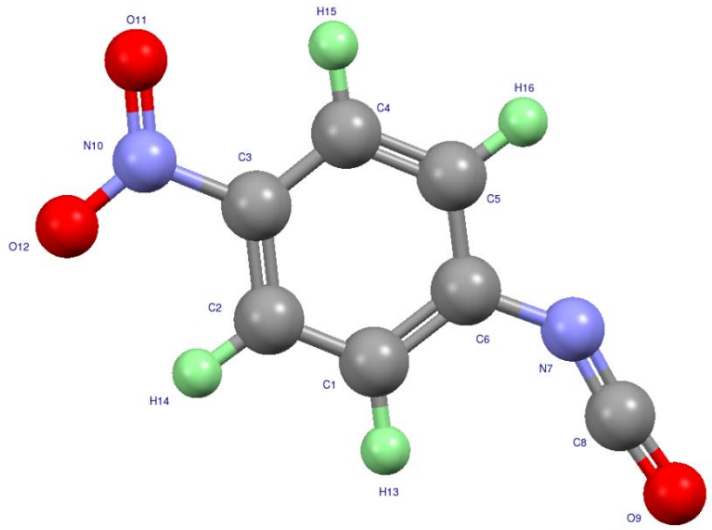

Figure 1. The optimized geometric structure of the NPIC molecule with atoms numbering scheme obtained by B3LYP/6–311++G (d, p) level of theory.

Table 1. DFT optimized bond length (Å)and bond angle (°) of NPIC molecule.

Number	Atom1	Atom2	Length (Å)	Atom1	Atom2	Atom3	Angle (°)
1	C1	C2	1.3865	C2	C1	C6	119.98
2	C1	C6	1.4032	C1	C2	C3	119.06
3	C2	C3	1.3923	C2	C3	C4	121.76
4	C3	C4	1.3918	C2	C3	N10	119.07
5	C3	N10	1.4754	C4	C3	N10	119.16
6	C4	C5	1.387	C3	C4	C5	119.04
7	C5	C6	1.4002	C4	C5	C6	120.07
8	C6	N7	1.3922	C1	C6	C5	120.09
9	N7	C8	1.2067	C1	C6	N7	121.86
10	C8	O9	1.1665	C5	C6	N7	118.05
11	N10	O11	1.2249	C6	N7	C8	139.34
12	N10	O12	1.2251	N7	C8	O9	173.6
				C3	N10	O11	117.63
				C3	N10	O12	117.63
				O11	N10	O12	124.74

The highest occupied molecular orbitals (HOMO) and the lowest unoccupied molecular orbitals (LUMO) are important parameters in quantum chemistry. The calculated frontier molecular orbital profile of the NPIC molecule is displayed in Figure 2. The HOMO indicates for the ability to donate an electron, and LUMO acts as an electron acceptor. The figure shows that the HOMO and LUMO are spread over the entire molecule. The red color indicates the positive phase, and the green color indicates the negative phase. In the molecular orbitals of NPIC, the HOMO and LUMO are located over the NPIC molecule except for nitrogen of the isocyanate group. HOMO-1 and LUMO+1 are the second-highest occupied and second-lowest unoccupied molecular orbitals, respectively. The HOMO-LUMO energy gap (Eg) of the title molecule is 4.516 eV, which is significantly affected the stability and reactivity of the molecule. The global parameters such as ionization potential, electron affinity, chemical potential, chemical hardness, electronegativity, electrophilicity, global softness are listed in table 2. The intermolecular interaction and molecular features of the system which strongly influence the binding of a substrate to its active sites are investigated using the MEP map (Figure 2). The map of NPIC gives a spectral display of increasing potential value from red to blue. The potential value ranges from −4.475e-2 a.u. (red) to +4.475e-2 a.u. (blue) for the molecule. The electrophilic attack is supported by the negatively active region (red) in NPIC, mainly distributed on oxygen atoms of nitro groups. . The blue regions are mainly distributed on the

hydrogen atoms of the isocyanate and benzene groups. The result indicates that the molecule reactive regions may interact with neighboring molecules.

Table 2. The energy and related quantum chemical parameters values of NPIC.

Parameters	Values
EHOMO (HF)	-0.28078
ELUMO (HF)	-0.11482
EHOMO (eV)	-7.6405854
ELUMO (eV)	-3.1244818
Energy gap (Δ) (eV)	4.51610352
Ionization energy (I) (eV)	7.64058536
Electron affinity (A) (eV)	3.12448184
Electronegativity (χ) (eV)	5.3825336
Chemical potential (μ) (eV)	-5.3825336
Global hardness (η) (eV)	2.25805176
Global softness (s) (eV-1)	0.44285964
Electrophilicity index (ω) (eV)	6.34151912

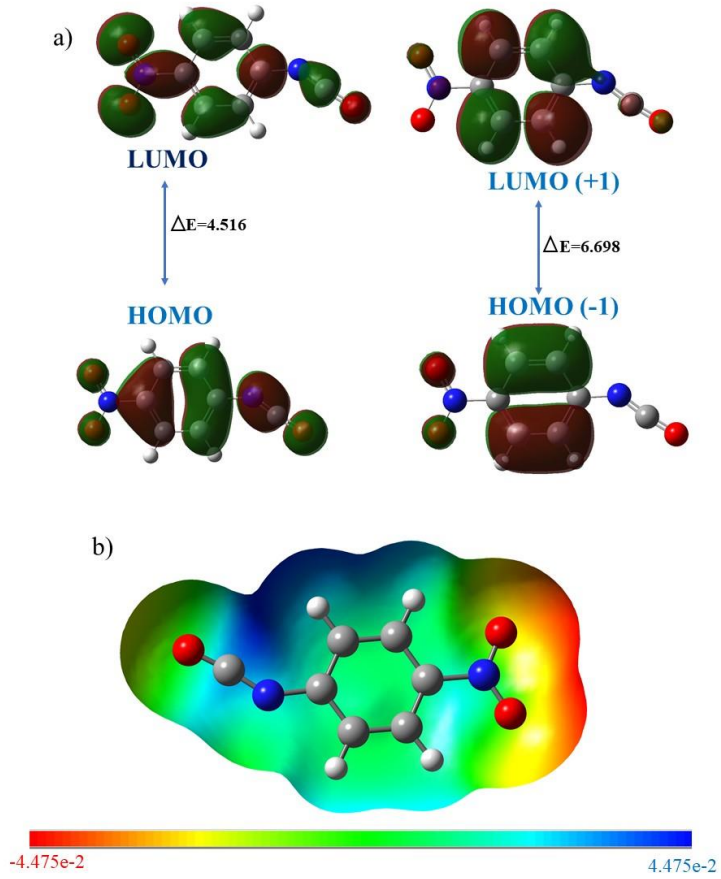

Figure 2. (a) Calculated frontier molecular orbital profile and **(b)** graphical view of the molecular electrostatic potential (MEP) map.

3.2. Electronic spectra of NPIC molecule.

TD-DFT/CAM-B3LYP 6-311G++(d,p) calculations were performed to study the electronic transitions of NPIC. The absorption spectra were recorded in the gas phase represented in Figure 3. Computed UV–visible spectrum exhibited intense allowed n-π*transition of maximum absorption observed at 295 nm. The lower UV cut-off wavelength is around 345 nm. Eg =1240/(nm) eV is used to compute the molecule's optical band gap energy, where λ is the lower cut-off wavelength (345 nm). The bandgap of the molecule is found to be 3.59 eV.

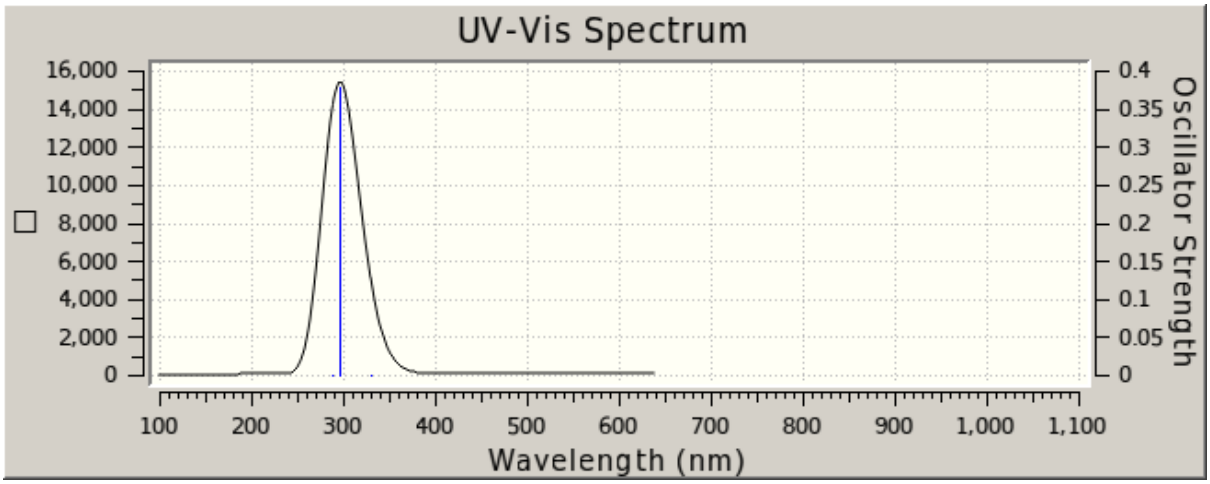

Figure 3. Simulated UV–visible absorption spectra for the title compound computed at B3LYP/6-311++ G (d, p) basis set.

3.3. Vibrational investigation of the title compound.

In the frequency range 3500 to 0 cm^{-1}, the calculated FT-IR spectrum of the title molecule was computed using the DFT/B3LYP/6-311G++(d,p) in the gaseous state. (Figure 4), and the vibrational assignments corresponding to their frequencies were carried out using the Gaussian 16 program. The intense peak was observed at 2357 due to the N=C=O stretching frequency. The peak is observed at 1354 and 1565 due to N-O symmetric (NO_2) and N-O asymmetric stretching frequency.

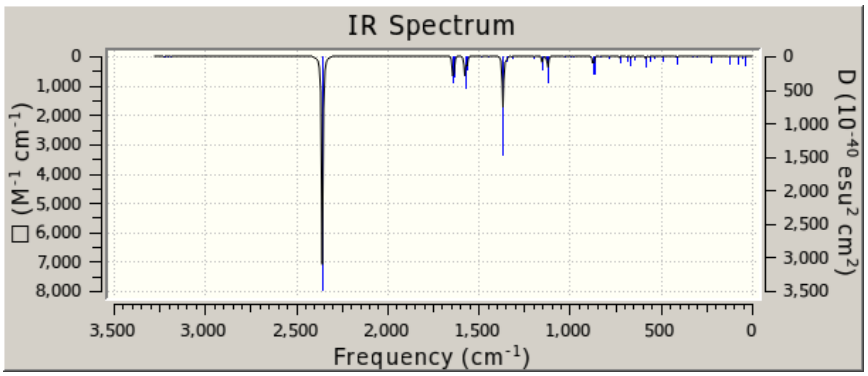

Figure 4. B3LYP/6-311++G(d,p) vibrational spectra of the title compound (cm^{-1}).

3.4. Toxicity.

By using a pkCSM tool, we can predict the toxicity of the molecules. The toxicity results of the title compound are interpreted. Due to the presence of cyanate group in the title molecule, the compound shows an AMES toxic nature, and also compounds are showing a high Maximum tolerated dose for humans. The oral rat acute and chronic toxicity were also studied, and results were interpreted. Hepatotoxicity and Skin Sensitization of the compound were studied, and the results are shown in Table 3. In minnow toxicity compound shows a low acute toxicity nature.

Table 3. Toxicity by using pkCSM tool.

Parameters		**NPIC**
Toxicity	AMES toxicity	Yes
	Max. tolerated dose (human) (log mg/kg/day)	0.697

Parameters		NPIC
	hERG I inhibitor	No
	hERG II inhibitor	No
	Oral Rat Acute Toxicity (LD50) (mol/kg)	2.416
	Oral Rat Chronic Toxicity (LOAEL) (log mg/kg_bw/day)	1.556
	Hepatotoxicity	No
	Skin Sensitisation	Yes
	T. Pyriformis toxicity (log ug/L)	0.803
	Minnow toxicity (log mM)	1.262

3.5. Reduced density gradient (RDG) analysis.

Bader's theory (QTAIM), which is based on electron density topology, has recently emerged as a useful tool for analyzing a wide range of chemical interactions [19]. They include ionic, covalent, and hydrogen bonding, as well as relativistic interactions. QTAIM is now being used more often to examine weaker, more difficult-to-understand interactions, such as metal-metal or van der Waals interactions [20]. The electron density distribution of a molecule can be used to identify and analyze the ability and nature of intramolecular interactions. The Bader's theory QTAIM framework of NPIC disclose the presence of strong repulsions are in the six-membered rings, and van der Waals interactions happened between H15—O11 and H14—O12 atoms is shown in Figure 5. The interaction strength is represented by the graph of RDG versus electron density. The sign (λ_2) is used to differentiate between bonding (λ_2<0) and non-bonding (λ_2>0) interactions. The three-dimensional isosurface representation and two-dimensional RDG graphs are shown in Figure 7. The peaks at the positive sign (λ_2)>0.01 a.u on the 2D plot correspond to the red-colored isosurfaces, which reflect the strong repulsion or steric effect present in the molecules. Also, the green-colored isosurfaces correspond to the peaks at the values near zero and signify the weak interaction presented in the molecule, which indicates the less electronegative nature of the oxygen atom.

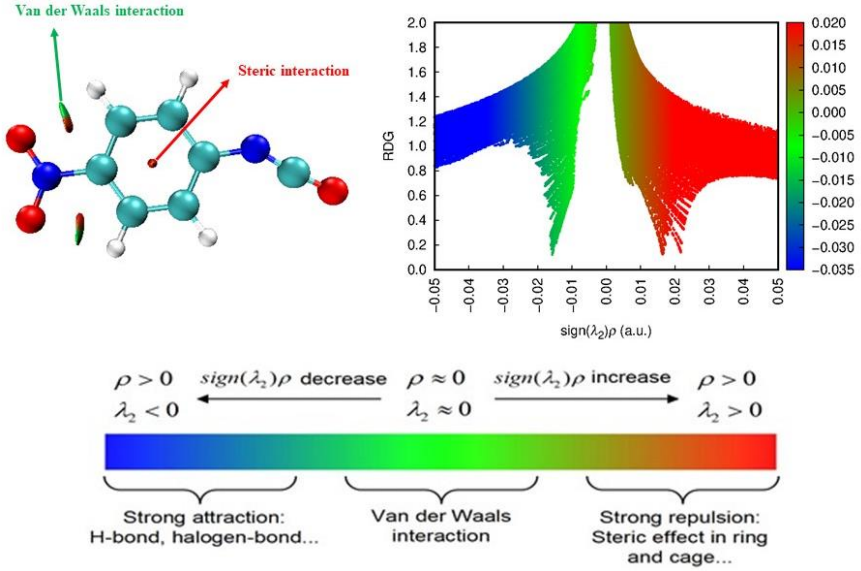

Figure 5. 3D non-covalent interactions and 2D scatter plot of NPIC with an isosurface value of 0.5.

3.6. Electron charge density distribution.

In various guest complexes, QTAIM theory may provide a much better and deeper understanding of chemical bond properties and the study of weak interactions [21]. In addition,

various QTAIM parameters may be used to efficiently quantify both weak interactions and chemical bonds are described based on critical bond point (BCP), electron density (ρ BCP), Laplacian (∇^2ρBCP), the bond ellipticity at BCP (ε), and total electronic energy density (HBCP). Higher electron density at BCPs implies high structural stability. The electron density is associated with bond strength or bond order; the nature of the interaction is reflected in the Laplacian and overall energy density. For covalent bonds, the value of the BCP is large, and the Laplacian is always negative. Still, for Vander Waals interactions, the value at the BCP is considerably smaller. Laplacian is always positive [22]. Two-dimensional contour line maps of Laplacian electron density and electron density of NPIC are shown in Figures 6a and 6b. This plot reveals that the inter-atomic regions, places of local charge concentration (dotted contour lines) appear and accumulate around the oxygen and nitrogen atoms, showing the ionic character of O-N and C-O bonds is higher than almost any other area. Because when the charge density is localized in the valence shell, the charge density is strongly connected and polarised. Figure 6c shows the relief maps of NPIC. Figure 6d shows the contour line map of NPIC, indicating that the negatively active region (red) is majorly spread on oxygen atoms of nitro groups supports the electrophilic attack. The blue regions are largely distributed on the hydrogen atoms of the isocyanate and benzene groups.

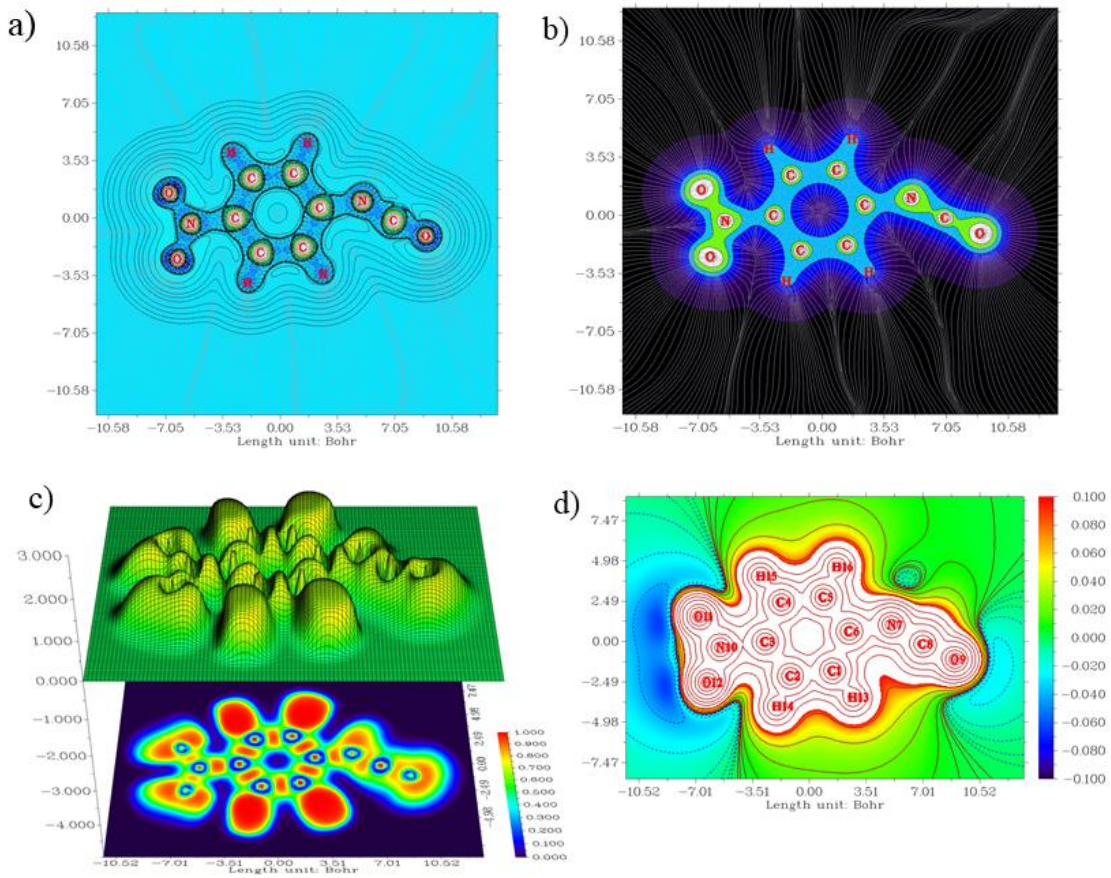

Figure 6. Quantum theory of atoms in the molecule (QTAIM analysis) [NPIC]: **(a)** contour line plots of the Laplacian of electron density (∇ 2 ρ), regions of charge-concentration (dotted lines in blue, ∇ 2 ρ < 0) and charge-depletion (solid lines in red, ∇ 2 ρ > 0), **(b)** contour line plots of the electron density (ρ), **(c)** surface maps of electron localization function (ELF) and the value of ELF is given by the color scale, **(d)** contour line plot of electrostatic potential (ESP).

4. Conclusions

In the present study, we have successfully optimized the structure of the title compound (4-nitro phenyl isocyanate). The title compound was subjected to theoretical studies such as

FT-IR and UV-visible spectra. Its optimized molecular structure was obtained by the DFT-B3LYP method at the level of 6311++G(d,p). The UV-visible bandgap energy obtained by theoretical was found to be 3.59 eV. The calculated HOMO-LUMO energy gap is 4.516 eV. The MEP map was traced, and the chemical activity of the title molecule was noticed. The title compound obeys the all-limitations toxicity property, and RDG analysis reveals the presence of weak interactions, strong attractions, and strong repulsions in the title compound.

Funding

This research was funded by SJCE, JSS Science and Technology University, and VGST-CISEE Project (GRD 647), GOK, Karnataka.

Acknowledgments

The authors are thankful to SJCE, JSS Science and Technology University, and VGST-CISEE Project (GRD 647), GOK, Karnataka.

Conflicts of Interest

The authors declare no conflict of interest.

References

1. Taheri-Ledari, R.; Mirmohammadi, S.S.; Valadi, K.; Maleki, A.; Shalan, A.E. Convenient conversion of hazardous nitrobenzene derivatives to aniline analogues by Ag nanoparticles, stabilized on a naturally magnetic pumice/chitosan substrate. *RSC Advance.* **2020**, *10*, 43670-43681, https://doi.org/10.1039/D0RA08376C.
2. Chakraborty, S.; Mruthunjayappa, M.H.; Aruchamy, K.; Singh, N.; Prasad, K.; Kalpana, D.; Ghosh, D.; SannaKotrappanavar, N.; Mondal, D. Facile Process for Metallizing DNA in a Multitasking Deep Eutectic Solvent for Ecofriendly C–C Coupling Reaction and Nitrobenzene Reduction. *ACS Sustainable Chemistry & Engineering.* **2019**, *7*, 14225-14235, https://doi.org/10.1021/acssuschemeng.9b03224.
3. Kumar, K.P.; Kalla, R.M.N.; Varalakshmi, M.; Venkataramaiah, C.; Kumari, K.S.; Kannali, J.; Reddy, D.V.; Nagaraju, C. Synthesis, spectral characterization, antimicrobial activity and docking studies against DNA Gyrase-A of new 4-chloro-3-nitrobenzene sulfonamide derivatives. *Organic Communications* **2020**, *13*, 164, http://doi.org/10.25135/acg.oc.90.20.11.1858.
4. Rahimi, J.; Taheri-Ledari, R.; Niksefat, M.; Maleki, A. Enhanced reduction of nitrobenzene derivatives: Effective strategy executed by Fe3O4/PVA-10% Ag as a versatile hybrid nanocatalyst. *Catal. Commun* **2020**, *134*, 105850, https://doi.org/10.1016/j.catcom.2019.105850. ,
5. Zamli, K.M.; Asari, A.; Hashim, F.; Yusoff, H.M.; Mohamad, H.; Abdullah, F. Anti-Amoebic Activity of Eugenol Derivatives against Acanthamoeba castellanii. *Malaysian Journal of Chemistry* **2020**, *22*, https://ikm.org.my/ojs/index.php/MJChem/article/view/679.
6. Li, D.; Schwabedissen, J.; Stammler, H.G.; Mitzel, N.W.; Willner, H.; Zeng, X. Dichlorophosphanyl isocyanate–spectroscopy, conformation and molecular structure in the gas phase and the solid state. *Phys. Chem. Chem. Phys.***2016**, *18*, 26245-26253, https://doi.org/10.1039/c6cp05377g.
7. Varthya, S.B.; Sarma, P.; Bhatia, A.; Shekhar, N.; Prajapat, M.; Kaur, H.; Thangaraju, P.; Kumar, S.; Singh, R.; Siingh, A.; Prakash, A. Efficacy of green tea, its polyphenols and nanoformulation in experimental colitis and the role of non-canonical and canonical nuclear factor kappa beta (NF-kB) pathway: a preclinical in-vivo and in-silico exploratory study. *J. Biomol. Struct. Dyn.* **2021**, *39*,5314-5326, https://doi.org/10.1080/07391102.2020.1785946.
8. Zapata-Morales, J.R.; Pérez-González, C.; Alonso-Castro, A.J.; Martell-Mendoza, M.; Hernández-Munive, A.; Pérez-Gutiérrez, S. Synthesis and evaluation of antinociceptive and anti-inflammatory effects of nitro-porphyrins. *Med. Chem. Res.* **2018**, *27*,1782-1791, https://link.springer.com/article/10.1007/s00044-018-2191-z.
9. Anusuya, N.; Pragathiswaran, C.; Mary, J.V. A potential catalyst-TiO2/ZnO based chitosan gel beads for the

reduction of nitro-aromatic compounds aggregated sodium borohydride and their antimicrobial activity. *J. Mol. Struct.* **2021**, *1236*, 130197, https://doi.org/10.1016/j.molstruc.2021.130197.
10. Lee, H.; Cho, S.; Lee, Y.; Jung, B. Stereoselective Formal Hydroamidation of Si-Substituted Arylacetylenes with DIBAL-H and Isocyanates: Synthesis of (E)-and (Z)-α-Silyl-α, β-unsaturated Amides. *J. Org. Chem.* **2020**, *85*, 12024-12035, https://doi.org/10.1021/acs.joc.0c01903.
11. Vazaios, A.; Touris, A.; Echeverria, M.; Zorba, G.; Pitsikalis, M. Micellization behaviour of linear and nonlinear block copolymers based on poly (n-hexyl isocyanate) in selective solvents. *Polymers.* **2020**, *12*,1678, https://doi.org/10.3390/polym12081678.
12. Lv, Z.J.; Wei, J.; Zhang, W.X.; Chen, P.; Deng, D.; Shi, Z.J.; Xi, Z. Direct transformation of dinitrogen: synthesis of N-containing organic compounds via N− C bond formation. *Natl. Sci. Rev.* **2020**, *7*, 1564-1583, https://doi.org/10.1093/nsr/nwaa142.
13. Chrostowska, A.; Darrigan, C.; Dargelos, A.; Graciaa, A.; Guillemin, J.C. Isoselenocyanates versus isothiocyanates and isocyanates. *Phys. Chem. A.* **2018**, *122*, 2894-2905, https://doi.org/10.1021/acs.jpca.7b12604.
14. El Bakri, Y.; Ramli, Y.; Essassi, E.M.; Mague, J.T. Synthesis, crystal structure, spectroscopic characterization, Hirshfeld surface analysis, and DFT calculations of 1, 4-dimethyl-2-oxo-pyrimido [1, 2-a] benzimidazole hydrate. *J. Mol. Struct.* **2018**, *1152*, 154-162, https://doi.org/10.1016/j.molstruc.2017.09.074.
15. Chandini, K.M.; Al-Ostoot, F.H.; Shehata, E.E.; Elamin, N.Y.; Ferjani, H.; Sridhar, M.A.; Lokanath, N.K. Synthesis, crystal structure, Hirshfeld surface analysis, DFT calculations, 3D energy frameworks studies of Schiff base derivative 2, 2′-((1Z, 1′ Z)-(1, 2-phenylene bis (azanylylidene)) bis (methanylylidene)) diphenol. *J. Mol. Struct.* **2021**, *1244*, 130910, https://doi.org/10.1016/j.molstruc.2021.130910.
16. Usman, M.; Khan, R.A.; Alsalme, A.; Alharbi, W.; Alharbi, K.H.; Jaafar, M.H.; Abu Khanjer, M.; Tabassum, S. Structural, Spectroscopic, and Chemical Bonding Analysis of Zn (II) Complex [Zn (sal)](H2O): Combined Experimental and Theoretical (NBO, QTAIM, and ELF) Investigation. *Crystals.* **2020**, *10*, 259, https://doi.org/10.3390/cryst10040259.
17. Nanjundaswamy, S.; Hema, M.K.; Karthik, C.S.; Rajabathar, J.R.; Arokiyaraj, S.; Lokanath, N.K.; Mallu, P. Synthesis, crystal structure, in-silico ADMET, molecular docking and dynamics simulation studies of thiophene-chalcone analogues. *J. Mol. Struct.* **2022**, *1247*, 131365, https://doi.org/10.1016/j.molstruc.2021.131365.
18. Gurumallappa, G.; Jayashankar, J.; Puttaswamy, A.; Sunderraj, J.; Mallu, P.; Beeregowda, K. 4-(tert-butyl)-N, N-diethylbenzenesulfonamide: Structural, absorption distribution metabolism excretion toxicity (ADMET) and molecular docking studies. *Curr. Chem. Lett*. **2021**, *10*, 329-336, http://dx.doi.org/10.5267/j.ccl.2021.3.004.
19. Wu, L.C.; Thomsen, M.K.; Madsen, S.R.; Schmoekel, M.; Jørgensen, M.R.; Cheng, M.C.; Peng, S.M.; Chen, Y.S.; Overgaard, J.; Iversen, B.B. Chemical Bonding in a Linear Chromium Metal String Complex. *Inorg.* **2018**, *53*,12489-12498, https://doi.org/10.1021/ic501603x.
20. Bader, R.F.; Matta, C.F. Bonding to titanium. *Inorg.* **2001**, *40*, 5603-5611, http://alpha.chem.umb.edu/chemistry/Seminar/01-08%20WQE/Inorg%20Chem%20I%20Article%202008.pdf.
21. Bader, R.F.; Essén, H. The characterization of atomic interactions. *J. Chem. Phys.* **1984**, *80*, 1943-1960, https://doi.org/10.1063/1.446956.
22. Cremer, D.; Kraka, E. Chemical bonds without bonding electron density—does the difference electron-density analysis suffice for a description of the chemical bond?. *Angew. Chem. Int. Ed.* **1984**, *23*, 627-628, https://doi.org/10.1002/anie.198406271.